Mid-infrared Self-Similar Pulse Compression in a Tapered Tellurite Photonic Crystal Fiber and Its Application in Supercontinuum Generation

Feng Xu, Jinhui Yuan, *Member*, *IEEE*, *Member*, *OSA*, Chao Mei, Feng Li, Zhe Kang, Binbin Yan, Xian Zhou, Qiang Wu, Kuiru Wang, Xinzhu Sang, Chongxiu Yu, and Gerald Farrell

***Abstract*—In this paper, we design a tapered tellurite photonic crystal fiber (TTPCF) with nonlinear coefficient increasing along the propagation direction, and demonstrate the mid-infrared self-similar pulse compression of the fundamental soliton in such a TTPCF. When the variation of group-velocity dispersion, higher-order dispersion, higher-order nonlinearity, and linear loss are considered, a 1 ps pulse at wavelength 2.5 μm can be compressed to 62.16 fs after a 1.63-m long propagation, along with the negligible pedestal, compression factor F_c of 16.09, and quality factor Q_c of 83.16%. Then the compressed pulse is launched into another uniform tellurite PCF designed, and highly coherent and octave-spanning supercontinuum (SC) is generated. Compared to the initial picosecond pulse, the compressed pulse has much larger tolerance of noise level for the SC generation. Our research results provide a promising solution to realize the fiber-based mid-infrared femtosecond pulse source for nonlinear photonics and spectroscopy.**

***Index Terms*—Tapered tellurite photonic crystal fiber, self-similar pulse compression, SC generation.**

I. Introduction

THE ultrashort pulses can find important applications in supercontinuum (SC) generation, frequency comb generation, biological imaging, and optical communication [1]-[4], etc. Over the past few years, several pulse compression methods were used to generate the ultrashort pulses in different nonlinear media. For adiabatic soliton compression in dispersion-decreasing fibers (DDFs) or tapered photonic crystal fibers (TPCFs) [5]-[7], large compression factor was obtained, but the fiber lengths were too long to meet the need of miniaturization. For higher-order soliton compression, large compression factor can be achieved within short nonlinear media [8]-[11], but it will generate large pedestal, which significantly limits its application in laser and telecommunication systems. In contrast, the self-similar pulse compression is an effective method for obtaining highly compressed pulse without pedestals within short nonlinear media [2], [8], [12]-[17]. In 2005, Méchin *et al.* obtained a compression factor over 20 with self-similar propagation of a pulse in a DDF amplifier [12]. In 2006, Méchin *et al.* investigated the self-similar propagation in a comblike DDF amplifier and obtained a compression factor of 12 [13]. In 2013, Li *et al.* theoretically demonstrated the self-similar pulse compression in nonlinear fiber Bragg gratings (NFBGs) [14] and the effect of third-order dispersion was further discussed [15]. In 2014, Li *et al.* reported the self-similar pulse compression in a nonlinearity increasing silica PCF taper with a length of 6.42 m [2]. The self-similar pulse compression was introduced to on-chip system with a theoretical demonstration in a chalcogenide-silicon slot waveguide taper in 2016 [8]. It should be noted that all above schemes are proposed to work in near-infrared region.

The demand of pulse compression in mid-infrared region is much stronger than that in near-infrared region due to the lack of mid-infrared ultrashort pulsed laser sources. The nonlinear phenomena including soliton self-frequency shift, SC generation, wavelength conversion, and harmonic generation have attracted much interest in recent years [18-20]. Among these phenomena, SC generation is the most complex nonlinear optical phenomenon [21]-[25], which is resulted from the interplay of some nonlinear effects, including self-phase modulation (SPM), modulation instability (MI), stimulated Raman scattering (SRS), and soliton dynamics [26]-[29], etc. In practice, SC generation is the enabling technique to realize self-referenced frequency comb sources. However, highly coherent octave spanning SC is hard to be obtained without femtosecond pump pulses in anomalous dispersion region due to dominant MI and uncontrollable soliton fission [21], [24].

Manuscript received at

Supported by the National Natural Science Foundation of China (61475023 and 61475131), Beijing Youth Top-notch Talent Support Program (2015000026833ZK08), Fund of State Key Laboratory of Information Photonics and Optical Communications (Beijing University of Posts and Telecommunications) P. R. China (IPOC2016ZT05 and IPOC2017ZZ05), Shenzhen Science and Technology Innovation Commission (JCYJ20160331141313917) and Research Grant Council of Hong Kong (PolyU152144/15E). (The corresponding authors: Jinhui Yuan and Feng Li, e-mails: yuanjinhui81@bupt.edu.cn, enlf@polyu.edu.hk).

Feng Xu, Jinhui Yuan, Chao Mei, Binbin Yan, Kuiru Wang, Xinzhu Sang, and Chongxiu Yu are with the State Key Laboratory of Information Photonics and Optical Communications, Beijing University of Posts and Telecommunications (BUPT), Beijing, P. R. China.

Jinhui Yuan, Feng Li, Zhe Kang, and Xian Zhou are with the Photonics Research Centre, Department of Electronic and Information Engineering, the Hong Kong Polytechnic University, Hung Hom, Hong Kong.

Feng Li is also with the Hong Kong Polytechnic University Shenzhen Research Institute, 518057, Shenzhen, P. R. China.

Qiang Wu is with the Department of Physics and Electrical Engineering, Northumbria University, Newcastle upon Tyne, NE1 8ST, United Kingdom.

Gerald Farrell is with Photonics Research Centre, Dublin Institute of Technology, Dublin, Ireland.

Self-similar pulse compression will be the enabling technique to obtain highly coherent SC with a picosecond pump pulse [2].

To obtain the self-similar pulse compression in mid-infrared region, we have proposed an inversely tapered silicon ridge waveguide in 2017 [16]. Recently, a tapered tellurite PCF (TTPCF) was also investigated to realize mid-infrared self-similar pulse compression [17]. Tellurite glass has a much higher nonlinear refractive index (10-50$\times$ 10^{-20} m^2/W) than silica. Furthermore, tellurite glass is chemically and thermally stable than other non-silica glasses [30]-[31]. Therefore, tellurite glass can be considered as suitable fiber material for investigating both the self-similar pulse compression and SC generation.

In this paper, we demonstrate the mid-infrared self-similar pulse compression of the fundamental soliton in a TTPCF designed with nonlinear coefficient increasing along the propagation direction. A 1 ps pulse at wavelength 2.5 μm is successfully compressed to 62.16 fs. Then we launch the compressed pulse into another uniform tellurite PCF designed, and highly coherent and octave-spanning SC is generated.

II. Theoretical Model

The pulse propagation in the TTPCF can be described by generalized nonlinear Schrödinger equation (GNLSE) as [2], [24], [32]

$$\frac{\partial A}{\partial z}+\frac{\alpha_0}{2}A-\sum_{m\geq 2}\frac{i^{m+1}\beta_m(z)}{m!}\frac{\partial^m A}{\partial t^m}=i\gamma(z) \times\left(1+\tau_{shock}\frac{\partial}{\partial t}\right)\times\left[A(z,t)\int_0^{\infty}R(t')\left|A(z,t-t')\right|^2 dt'\right], \quad (1)$$

where $A(z, t)$ represents the slowly varying envelope, α_0 is the linear loss, $\beta_m(z)$ (m = 2, 3,…, and 12) is m-order dispersion coefficient at propagation distance z and calculated from Taylor expansion of the propagation constant $\beta(\omega)$ at a specific wavelength. $\gamma(z)$ is the Kerr nonlinear coefficient, which can be calculated by integration over the whole cross-section of the tellurite PCF as [12], [33]

$$\gamma=\frac{2\pi}{\lambda}\frac{\iint n_2(x,y)\left|F(x,y)\right|^4 dxdy}{\left(\iint\left|F(x,y)\right|^2 dxdy\right)^2}, \quad (2)$$

where $n_2(x, y)$ is nonlinear refractive index and $F(x, y)$ represents the distribution of the electric field. Nonlinear dispersion τ_{shock} = $\gamma_1(\omega_0)/\gamma(\omega_0)$ corresponds to the effect of self-steeping (SS), where $\gamma_1(\omega)$ = d$\gamma(\omega)$/dω and ω_0 is the central angular frequency. $R(t)$ denotes the nonlinear response function which includes the Kerr and delayed Raman responses.

As reported in Refs [34], [35], the self-similar solutions can be found in parameter-varying nonlinear Schrödinger equation (NLSE)

$$i\frac{\partial A}{\partial z}-\frac{\beta_2(z)}{2}\frac{\partial^2 A}{\partial t^2}+\gamma(z)\left|A\right|^2 A=0, \quad (3)$$

When the dispersion profile $\beta_2(z)$ is a constant and $\gamma(z)$ varies along the TTPCF as

$$\gamma(z)=\frac{\gamma(0)}{1-\sigma z}, \quad (4)$$

where $\sigma = \beta_2(0)\xi$ and ξ represents the initial chirp factor of the incident pulse. By taking Eq. (4) into Eq. (3), we can obtain a group of analytic self-similar solutions of Eq. (3) as [35]

$$A(t,z)=\left(\frac{P_0}{1-\sigma z}\right)^{1/2}\operatorname{sech}\left(\frac{t-t_0}{T_0(1-\sigma z)}\right)\exp\left(\frac{i\xi(t-t_0)^2}{2(1-\sigma z)}\right), \quad (5)$$

where the initial pulse peak power P_0 = $|\beta_2(0)|/(\gamma(0)T_0^2)$ is chosen to ensure the fundamental soliton propagation. T_0 is the initial pulse width, and t_0 is the temporal position of the pulse peak. From Eq. (5), the pulse width and peak power will decrease and increase along z when $\sigma z < 1$, respectively. Moreover, they vary along z as [2], [35]

$$T(z)=T(0)(1-\sigma z),\quad P(z)=\frac{P(0)}{1-\sigma z}. \quad (6)$$

III. Design of the TTPCF

In order to satisfy the self-similar compression condition, we design a TTPCF, which can be fabricated with tellurite glass ($75TeO_2$-$20ZnO$-$5Na_2O$ (mol.%), TZN, n_2 = 1.7×10^{-19} m^2/W) [36]-[38]. Fig. 1(a) shows the cross-section of the TTPCF. From Fig. 1(a), five rings of air-holes are arranged in a triangular lattice. At the input end, the hole to hole pitch Λ is chosen as 40 μm, and air-hole diameter d is 0.4Λ to ensure the single-mode propagation [39]. Fig. 1(b) shows the relationship between Λ and z. From Fig. 1(b), Λ gradually reduces as z increases. At the output end, Λ is reduced to 5.82 μm after a 1.63-m long propagation. Such a TTPCF with the length of 1.63 m can be drawn in fiber tower which have tapered a much longer length [7] rather than tapering machine. The inset of Fig. 1(b) shows a typical electrical field distribution calculated at wavelength 2.5 μm for Λ = 20 μm.

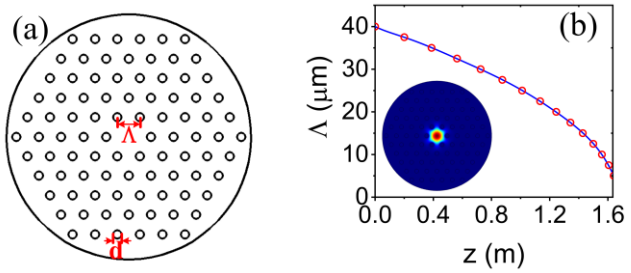

Fig. 1. (a) Cross-section of the TTPCF designed. (b) The relationship between the hole to hole pitch Λ and propagation distance z, the inset showing the typical electrical field distribution calculated at wavelength 2.5 μm for Λ =20 μm. The blue line is plotted by spline interpolation and the fitted Λ value is shown by the signed circles.

Figure 2(a) shows the calculated group-velocity dispersion β_2 versus wavelength for Λ varying from 2.35 to 2.65 μm. Λ changes from 5 to 40 μm with a step size of 5 μm. The dispersion curve decreases gradually along the increasing of Λ. The dispersion curves are almost linear in the considered spectral range for all Λ values. Fig. 2(b) shows the calculated group-velocity dispersion β_2 and nonlinear coefficient γ as functions of Λ, where the red circles correspond to the numerical results with full vector finite element method. From Fig. 2(b), both the variations of β_2 and γ are monotonic. As Λ reduces from 40 to 5.82 μm, γ and β_2 vary from 0.2 to 8.82 $W^{-1}km^{-1}$ and -92.2 to -148.73 ps^2/km, respectively. Compared

to the change of γ, the variation of β_2 can be negligible. The main reason is considered that for such a large mode area PCF, the light field is well confined in the core region and the material dispersion play an important role, so the waveguide dispersion induced by the variation of Λ has little influence on β_2. In contrast, γ varies evidently due to the change of effective mode area. According to Fig. 1(b), we can obtain the relationships between β_2 and γ and z, as shown in Fig. 2(c). At the output end of the TTPCF, the values of β_2 and γ are -148.73 ps^2/km and 8.82 W^{-1}km^{-1}, respectively.

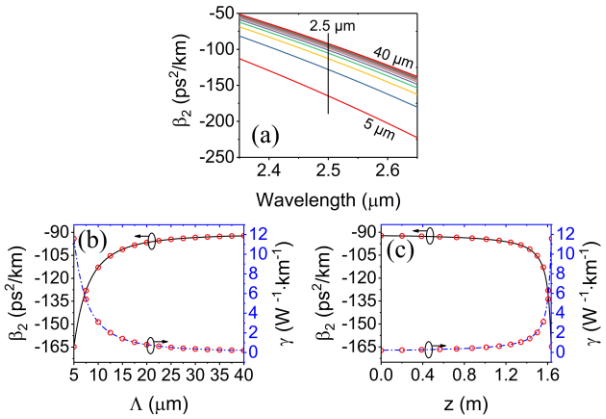

Fig. 2. (a) The calculated group-velocity dispersion β_2 versus wavelength for Λ varying from 2.35 to 2.65 μm. (b) and (c) present β_2 (black solid line) and nonlinear coefficient γ (blue dash dot line) at wavelength 2.5 μm versus Λ and z, respectively.

IV. Simulation Results and Discussion

In this work, a hyperbolic secant pulse with full width at half maximum (FWHM) of 1 ps is launched into the TTPCF. The chirp coefficient ξ is -6.5 ps^{-2}. In order to keep the fundamental soliton, the input peak power is chosen as 1.4 kW. The compression factor F_c and quality factor Q_c are used to evaluate the compression performance, which are respectively defined as [8], [40]

$$F_c = FWHM_{in} / FWHM_{out},\ Q_c = \frac{P_{out}}{P_{in}F_c}\times 100\%, \qquad (7)$$

where $FWHM_{in}$ and $FWHM_{out}$ represent the input and output FWHM, respectively. P_{in} and P_{out} are the peak powers of the input and output pulses. In the ideal case, the variation of the group-velocity dispersion $\beta(z)$, higher-order dispersion (HOD), higher-order nonlinearity (HON), and α_0 are neglected. The evolutions of the temporal and spectral profiles are shown in Figs. 3(a) and 3(b), respectively. It can be seen that both the temporal and spectral profiles are monotonous and symmetric. The peak power of the output pulse can be up to 60 kW, and the calculated F_c = 44.1 and Q_c = 1, respectively.

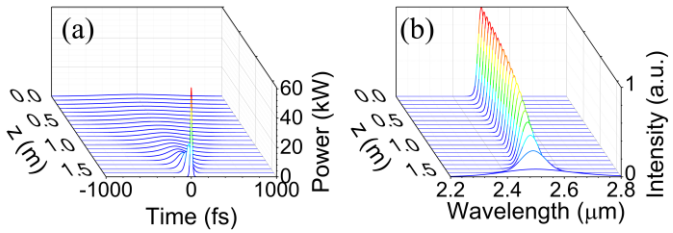

Fig. 3. (a) Temporal and (b) spectral evolutions along the 1.63-m long TTPCF for the ideal case (NLSE).

In the realistic case, the variation of $\beta(z)$, HOD, HON, and α_0 cannot be neglected, e.g. the case of GNLSE. Figs. 4(a) and 4(b) show the temporal and spectral profiles along the TTPCF when they are considered. The Raman response function of TZN is described as [41]

$$h_R(t) = \sum_{i=1}^{7} A_i \exp(-\gamma_i t)\exp(-\Gamma_i^2 t^2/4)\sin(\omega_{v,t} t), \qquad (8)$$

where γ_i, Γ_i, and $\omega_{v,t}$ represent the Lorentzian, Gaussian FWHM, and Gaussian component position. α_0 is chosen as 0.35 dB/m [38], [41]. From Fig. 4(a), the pulse width is reduced as the frequency shift and peak power P_0 increase. From Fig. 4(b), the corresponding spectrum intensity is reduced during the spectral broadening, and a small peak appears at the output end. By comparing Fig. 3 and Fig. 4, it can be found that the peak power of the output pulse is much lower and the corresponding FWHM is wider. A 1 ps input pulse can be compressed to 62.16 fs, and the peak power of the output pulse can be up to 18.78 kW, corresponding to F_c = 16.09 and Q_c = 83.16%.

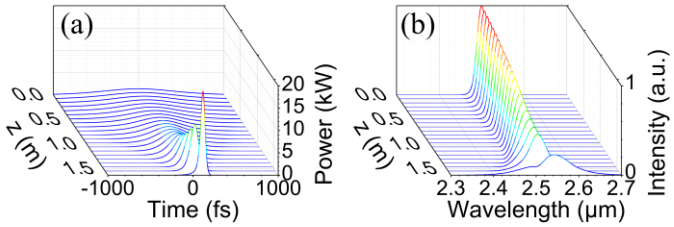

Fig. 4. (a) Temporal and (b) spectral evolutions along the 1.63-m long TTPCF for the realistic case (GNLSE).

Fig. 5(a) shows the relationships between the peak power P_0 and FWHM and z. When z < 1.5 m, P_0 gradually increases as z increases, as predicted by Eq. (6), and the FWHM almost changes linearly. However, when $z \geq$ 1.5 m, P_0 and FWHM begin to deviate from the original route, which is induced by the rapid variation of β_2 and breakdown of self-similar condition. In contrast, the increased γ can enhance the compression effect. Fig. 5(b) shows the dispersion length L_D and nonlinear length L_{NL} as functions of z. L_D and L_{NL} are defined as

$$L_D = \frac{T_0^2}{|\beta_2|},\ L_{NL} = \frac{1}{\gamma P_0}. \qquad (9)$$

In the process of the self-similar compression, L_D and L_{NL} are not exactly equal due to variation of $\beta(z)$ and α_0. When z < 1.48 m, L_D is slightly smaller than L_{NL}. L_D exceeds L_{NL} when $z \geq$ 1.48 m because γ increases rapidly and nonlinear effect will be enhanced. The difference between L_D and L_{NL} is less than 0.1, so we can consider that L_D and L_{NL} are approximately equal and the fundamental soliton can be well maintained during the self-similar propagation.

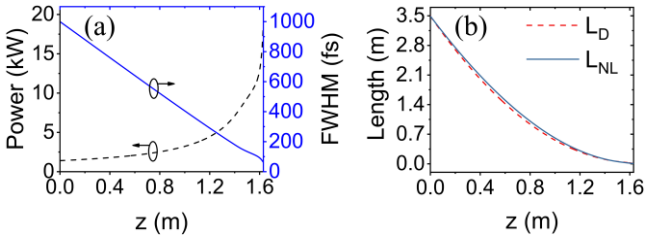

Fig. 5. (a) The peak power P_0 (blue solid line) and FWHM (black dashed line), and (b) L_D (red dashed line) and L_{NL} (blue solid line) as functions of z.

From Fig. 3(a) and Fig. 4(a), it can be seen that $FWHM_{out}$ in the realistic case is much wider than that of the ideal case since the self-similar pulse compression is deviated when variation of $\beta(z)$, HOD, HON, and α_0 are considered. To investigate the influence of each effect to perturb the self-similar pulse compression, we compare the output temporal and spectral profiles by considering them one by one. Figs. 6(a) and 6(b) show the temporal and spectral waveforms when variation of $\beta(z)$, HOD, HON, and α_0 are respectively considered. The ideal case is also given for comparison. From Figs. 6(a) and 6(b), when only variation of $\beta(z)$ is considered, the output pulse width is larger than that of the ideal case because the self-similar condition cannot be satisfied. If we only consider the HOD, the output spectrum shows asymmetry, along with a small peak, and the temporal waveform is delayed ~ 40 fs. When only considering the HON, the output spectrum is red-shifted about 110 nm due to intra-pulse Raman scattering. Moreover, the SS also causes asymmetry in both temporal and spectral waveforms. When only α_0 is considered, the peak power of the output pulse is decreased, and the pulse width keeps almost unchanged. When taking all effects into account, a 62.16 fs pulse with negligible pedestal can be obtained.

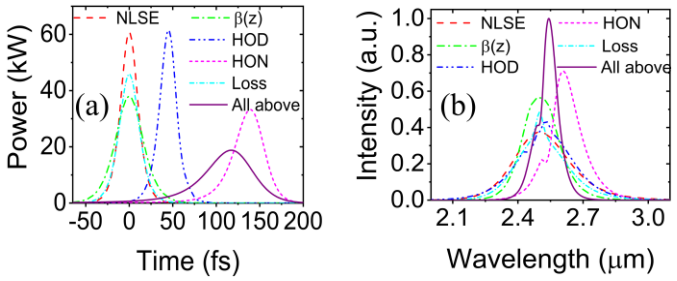

Fig. 6. (a) Temporal and (b) spectral profiles for the ideal case (NLSE, red dash line), $\beta(z)$ (green dash dot line), HOD (blue dash dot dot line), HON (magenta short dash line), α_0 (cyan short dash dot line) and all effects (purple solid line).

TABLE I
F_c AND Q_c FOR DIFFERENT CASES

Effects Considered	F_c	Q_c
NLSE	44.10	100%
$\beta(z)$	26.93	100%
HOD	45.17	97.27%
HON	25.46	93.30%
Loss	37.41	87.54%
All above	16.09	83.16%

Based on the temporal and spectral profiles shown in Fig. 6, we summarize F_c and Q_c for the different cases in Table I. From Table I, the varying dispersion $\beta(z)$ and HON are the dominant effects that decrease F_c. The impact of HOD is minor for both F_c and Q_c. The inclusion of loss introduces the most severe degradation of Q_c. For the TTPCF, the HOD, HON, linear loss, and non-constant β_2 are all perturbations to the self-similar compression. In the early stage of compression, the variation of β_2 is the dominant perturbation but the impacts of HOD and HON including self-steepening and Raman scattering will increase quickly along the compression of pulse.

From the above results, self-similar pulse compression can be well achieved in such a TTPCF without considering the random noise. However, the random noise is unavoidable in practice. In the following, we will investigate its impact. The random noise is defined as $\sigma = \eta\overline{N}\exp(i2\pi\overline{U})$, where the noise amplitude η = 0.01. $\overline{N}$ is a normally distributed random variable with the mean value of 0 and standard deviation of 1, and $\overline{U}$ is an uniformly distributed variable between 0 and 1 [2], [23]. Fig. 7(a) shows the input pulse with random noise level η = 0.01. From Fig. 7(a), many burrs appear on the whole temporal profile. After the propagation of 1.63 m, the burrs are reduced greatly, as shown in Fig. 7(b). Moreover, the pulse width is almost the same as that without the random noise. It can be concluded that the self-similar pulse compression has little sensitivity on the random noise.

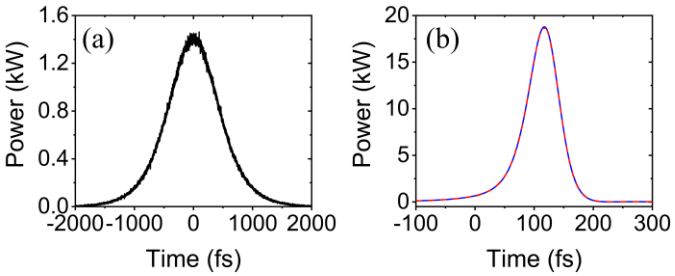

Fig. 7. (a) The 1 ps input pulse with the random noise, and (b) output pulse after self-similaer compression with (red dashed line) and without (black solid line) random noise.

V. HIGHLY COHERENT AND OCTAVE-SPANNING SC GENERATION

By using the shorter pulses (< 100 fs) as the input pump, the coherence of the SC can be evidently enhanced [2], [19], [20]. In the following, we will launch the self-similarly compressed pulse into another tellurite PCF designed for the SC generation.

Fig. 8(a) shows the cross-section of the uniform tellurite PCF designed. The fiber materials in the core and cladding region are chosen as TLWMN (TeO_2-Li_2O-WO_3-MoO_3-Nb_2O_3) and TZNL (TeO_2-ZnO-Na_2O-La_2O_3) [19], [42], respectively. For the TLWMN, n_2=5.9 × 10^{-19} m^2/W, and the Raman response function can be described as [19]

$$h_R(t) = \frac{\tau_1^2 + \tau_2^2}{\tau_1 \tau_2^2} \exp(-\frac{t}{\tau_2}) \sin(\frac{t}{\tau_1}), \qquad (10)$$

where Raman response time τ_1 = 7.4413 fs and τ_2 = 46.932 fs, respectively. The core diameter D of the tellurite PCF is 3.5 μm, and hole to hole pitch Λ is 5 μm. The first-ring hole diameter d_1 and second to fourth-rings hole diameter d_2 are chosen as 0.3Λ and 0.4Λ, respectively. The calculated curves of the group-velocity dispersion D and γ are shown in Fig. 8(b), where the inset shows the zoom-in dispersion curve in the wavelength range from 2.2 to 3.2 μm. From the inset of Fig. 8(b), the dispersion is very flat, which is beneficial for the SC generation. The value of γ is ~140.9 $W^{-1}km^{-1}$ at wavelength 2.5 μm.

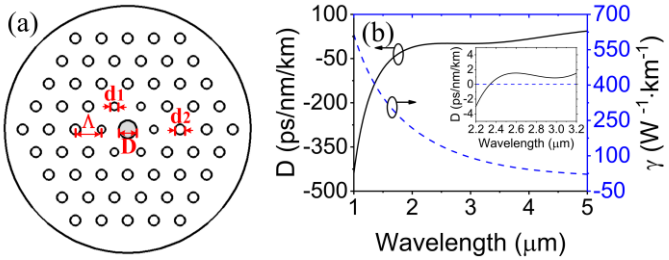

Fig. 8. (a) Cross-section of the tellurite PCF designed. (b) The group-velocity dispersion D (black solid line) and γ (blue dashed line) calculated as functions of the wavelength. The inset shows the zoom-in dispersion curve in the wavelength range from 2.2 to 3.2 μm.

When a 1 ps pulse at wavelength 2.5 μm with the peak power of 1.4 kW is launched into the tellurite PCF, the evolutions of the temporal and spectral profiles within a 0.55-m long propagation are shown in Fig. 9(a). From Fig. 9(a), the higher-order soliton occurs to spilt and the optical spectrum is rapidly broadened after propagation of ~0.35 m. The top figures in Fig. 9(a) show the output temporal and spectral profiles. We note that the output temporal profile has split into several pulses, and the fluctuation in output spectrum is obvious because of the MI and soliton fission, which introduce the noise and degrade the coherence of the SC.

By using the self-similarly compressed pulse of 62.16 fs with the peak power of 15.21 kW as the pump, the coupling problem between the TTPCF and the tellurite PCF can be solved with the method of fused biconical tapering [43]. In this case, the evolutions of the temporal and spectral profiles within a 5.5-cm long propagation are shown in Fig. 9(b). It can be seen from the top figures of Figs. 9(a) and 9(b) that for the 1 ps and 62.16 fs pulses, the output spectral widths are approximately the same, but the fiber length used is only tenth for the 62.16 fs pulse. Moreover, although soliton fission is observed during the propagation, the output spectrum is much smoother and flatter than that generated with the 1 ps pulse. Compared with Fig. 9(a), the temporal and spectral profiles are not sensitive to the noise seed since the MI is suppressed by the self-similar compression, and the coherence of the SC is greatly enhanced.

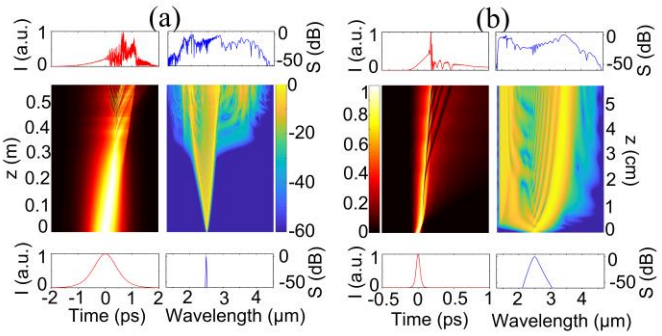

Fig. 9. The evolutions of temporal and spectral profiles of (a) the 1 ps pulse, and (b) the self-similarly compressed 62.16 fs pulse. The bottom and top figures show the temporal and spectral profiles at the input and output ends of the uniform tellurite PCF, respectively. I and S represent the intensity and spectrum, respectively.

To compare the coherence of the SCs generated with the 1 ps and 62.16 fs pulses, we use the degree of coherence $g_{12}^{(1)}$ to characterize the output spectra of the SC which is defined as [34], [44]-[45]

$$g_{12}^{(1)}(\lambda,t_1-t_2)=\left|\frac{\left\langle A_1^*(\lambda,t_1)\,A_2(\lambda,t_2)\right\rangle}{\left\langle\left|A_1(\lambda,t_1)\right|^2\right\rangle\left\langle\left|A_2(\lambda,t_2)\right|^2\right\rangle}\right|, \tag{11}$$

where $A(\lambda, t)$ represents the signal amplitude in the frequency domain. The angular brackets represent the ensemble average over independently pairs of spectra, i.e. $A_1(\lambda, t)$ and $A_2(\lambda, t)$, which are obtained from 50 shot-to-shot simulations with different random noises at wavelength λ. The random noise is defined above and we take $t_1 - t_2 = 0$. Moreover, it is necessary to weight $g_{12}^{(1)}$ in the whole spectrum as [2], [45]

$$R=\frac{\int_0^\infty g_{12}^{(1)}(\lambda,t_1-t_2)\cdot P(\lambda,t_1-t_2)d\lambda}{\int_0^\infty P(\lambda,t_1-t_2)d\lambda}, \tag{12}$$

where $P(\lambda,t)=\left\langle\left|A(\lambda,t)\right|^2\right\rangle$. In order to compare the slight difference of the coherence when they are close to 1, another variable K is introduced and defined as [2]

$$K=\lg(1-R). \tag{13}$$

We firstly investigate the coherence of the SC generated with 1 ps pump pulse. The input peak power and propagation length are chosen as 1.4 kW and 0.55 m, respectively. The spectra of the SC and $g_{12}^{(1)}$ calculated with the 50 shots with the random noise are shown in Figs. 10(a) and 10(c). The grey plots represent the overlapped spectra of the 50 shots with random noise level $\eta = 1 \times 10^{-3}$. From Fig. 10(a), the differences between the 50 shots are very large, so the corresponding $g_{12}^{(1)}$ is < 0.5 over the considered wavelength range, as shown in Fig. 10(c). In contrast, when the pulse of 62.16 fs with peak power of 15.21 kW is propagated inside a 5.5-cm long fiber, the overlapped spectra of the 50 shots with $\eta = 1 \times 10^{-3}$ represented by the grey plot are shown in Fig. 10(b), where the averaged spectrum of each 50 shots is plotted by the blue line. From Fig. 10(b), the spectral fluctuation decreases greatly. From Fig. 10(d), the corresponding $g_{12}^{(1)}$ is very close to 1 in the wavelength range of 1.5 to 4.5 μm. By comparing Fig. 10(c) and Fig. 10(d), it is concluded that highly coherent and octave-spanning SC can be generated with compressed pulse.

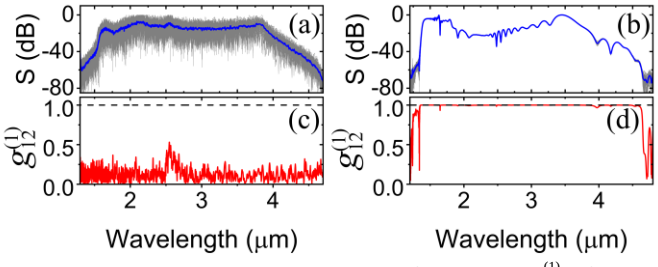

Fig. 10. (a) The spectra (S) and (c) degree of coherence $g_{12}^{(1)}$ of the SC generated with the 1 ps pulse with random noise level $\eta = 1 \times 10^{-3}$. (b) The spectra (S) and (d) $g_{12}^{(1)}$ of the SC generated with the 62.16 fs pulse with $\eta = 1 \times 10^{-3}$. The grey and blue lines in (a) and (b) represent the overlapped spectra of the 50 shots and average values of the 50 shots, respectively.

In order to quantitatively compare the coherence of the SC

generated with the 1 ps and 62.16 fs pulses, we calculate the weighted degree R for different lg(η) in the whole spectra, as shown in Fig. 11(a). For the 1 ps pulse, R is decreased with the increase of lg(η) and no more than 0.3 for all lg(η) values. When lg(η) = -9, R = 0.26, it can be drawn from the statistics that a very faint noise will seriously affect the output spectra. For compressed pulse of 62.16 fs, R is close to 1 when lg(η) ≤ -3. As lg(η) increases from -3 to -1, R drops quickly from 1 to 0.18. Especially, R begins to drop to be less than 0.5 when lg(η) = -1.6 ($\eta = 2.5 \times 10^{-2}$). In Fig. 11(b), K is also plotted since R is very close to 1 for the compressed pulse of 62.16 fs. K is increased with increase of lg(η) and several points are neglected if K < -7. For the 1 ps pulse, K is close to 0 when the value of $g_{12}^{(1)}$ is small. Therefore, the self-similar pulse compression can greatly suppress the random noise and improve the coherence of the SC.

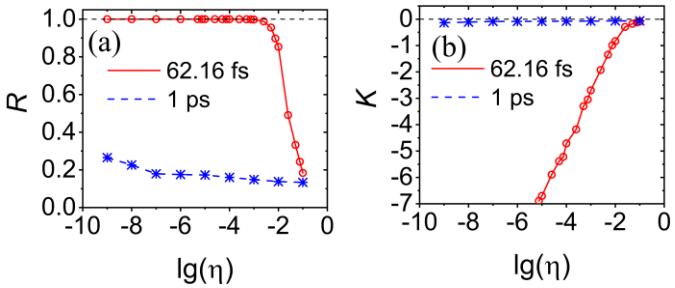

Fig. 11. The weighted degree of coherence (a) R and (b) K calculated in the whole spectra versus random noise level lg(η) for the SC generated with the 1 ps pulse (blue dashed star lines) and 62.16 fs pulse (red solid circle line).

VI. Conclusion

In summary, a TTPCF with increasing nonlinearity and comparatively unchanged dispersion is designed to achieve the self-similar pulse compression of the fundamental soliton. When the variation of $\beta(z)$, HOD, HON, and α_0 are considered, simulation results show that a 1 ps pulse at wavelength 2.5 μm can be self-similarly compressed to 62.16 fs, along with negligible pedestal. The corresponding F_c and Q_c are 16.09 and 83.16%, respectively. Then, another uniform tellurite PCF is designed for the SC generation. We launch the 1 ps pulse and compressed 62.16 fs pulse into the uniform tellurite PCF, respectively, it is found that the coherence of the SC generated with the compressed pulse is enhanced significantly compared to that generated with the 1 ps pulse, and highly coherent and octave-spanning SC can be obtained. It is believed that the proposed scheme provides a promising solution to realize the fiber-based mid-infrared femtosecond pulse source by using picosecond input pulse.

References

[1] J. H. Yuan, Z. Kang, F. Li, X. T. Zhang, X. Z. Sang, Q. Wu, B. B. Yan, K. R. Wang, X. Zhou, K. P. Zhong, G. Y. Zhou, C. X. Yu, C. Lu, H. Y. Tam, and P. K. A. Wai, "Mid-infrared octave-spanning supercontinuum and frequency comb generation in a suspended germanium-membrane ridge waveguide," *J. Lightwave Technol.*, vol. 35, no. 14, pp. 2994–3002, May. 2017.

[2] F. Li, Q. Li, J. H. Yuan, and P. K. A. Wai, "Highly coherent supercontinuum generation with picosecond pulses by using self-similar compression," *Opt. Express.*, vol. 22, no. 22, pp. 27339–27354, Nov. 2014.

[3] J. Rehbinder, L. Bruckner, A. Wipfler, T. Buckup, and M. Motzkus, "Mul-timodal nonlinear optical microscopy with shaped 10 fs pulses," *Opt. Express*, vol. 22, no. 23, pp. 28790–28797, Nov. 2014.

[4] J. M. Dudley and J. R. Taylor, "Chapter 6 Supercontinuum generation and nonlinearity in soft glass fibers," in *Supercontinuum Generation in Optical Fibers*, Cambridge, UK: Cambridge Univ. Press, 2010, pp. 82–119.

[5] M. D. Pelusi and H. F. Liu, "Higher order soliton pulse compression in dispersion-decreasing optical fibers," *IEEE J. Quantum Electron.*, vol. 33, no. 8, pp. 1430–1438, Aug. 1997.

[6] J. C. Travers, J. M. Stone, A. B. Rulkov, B. A. Cumberland, A. K. George, S. V. Popov, J. C. Knight, and J. R. Taylor, "Optical pulse compression in dispersion decreasing photonic crystal fiber," *Opt. Express.*, vol. 15, no, 20, pp. 13203–13211, Aug. 2007.

[7] M. L. V. Tse, P. Horak, J. H. V. Price, F. Poletti, F. He, and D. J. Richardson, "Pulse compression at 1.06 μm in dispersion-decreasing holey fibers," *Opt. Lett.*, vol. 31, no. 23, pp. 3504–3506, Dec. 2006.

[8] C. Mei, F. Li, J. H. Yuan, Z. Kang, X. T. Zhang, K. R. Wang, X. Z. Sang, Q. Wu, B. B. Yan, X. Zhou, L. Wang, C. X. Yu, and P. K. A. Wai, "High degree picosecond pulse compression in chalcogenide-silicon slot waveguide taper." *J. Lightwave. Technol.* vol. 34, no. 16, pp. 3843–3852, Aug. 2016.

[9] K. F. Mak, J. C. Travers, N. Y. Joly, A. Abdolvand, and P. St. J. Russell, "Two techniques for temporal pulse compression in gas-filled hollow-core kagomé photonic crystal fiber," *Opt. Lett.*, vol. 38, no. 18, pp. 3592–3595, Sept. 2013.

[10] Q. Li, J. N. Kutz, and P. K. A. Wai, "Cascaded higher-order soliton for non-adiabatic pulse compression," *J. Opt. Soc. Am. B.*, vol. 27, no. 11, pp. 2180–2189, Nov. 2010.

[11] K. C. Chan, "Short pulse generation by higher order soliton-effect compression: effects of optical fiber characteristics," *IEEE J. Quantum Electron.*, vol. 31, no. 12, pp. 2226–2235, Dec. 1995.

[12] D. Méchin, S. Im, V. Kruglov, and J. Harvey, "Experimental Demonstration of Self-Similar Pulse Compression and Amplification," presented at Nonlinear Guided Waves and Their Applications (NLGW), Dresden, Germany, Sep. 6-9, 2005.

[13] David Méchin, Sung-Hoon Im, Vladimir I. Kruglov, and John D. Harvey, "Experimental demonstration of similariton pulse compression in a comblike dispersion-decreasing fiber amplifier," *Opt. Lett.*, vol. 31, no. 14, pp. 2106-2108, Jul. 2006.

[14] Qian Li, P. K. A. Wai, K. Senthilnathan, and K. Nakkeeran, "Modeling Self-Similar Optical Pulse Compression in Nonlinear Fiber Bragg Grating Using Coupled-Mode Equations," *J. Lightwave Technol.*, vol. 29, no. 9, pp. 1293-1305, May. 2011.

[15] Q. Li, H. Huang, H. Lu, and S. Zhang, "Effects of Third-order Dispersion on Self-Similar Pulse Compression in Nonlinear Fibers," presented at Asia Communications and Photonics Conference (ACP), Beijing, China, Nov. 12-15, 2013.

[16] J. H. Yuan, J. Chen, F. Li, C. Mei, Z. Kang, X. T. Zhang, Y. Xu, B. B. Yan, X. Z. Sang, Q Wu, X Zhou, K. P. Zhong, K. R. Wang, C. X. Yu, Gerald Farrell, and P. K. A. Wai, "Mid-infrared self-similar compression of picosecond pulse in an inversely tapered silicon ridge waveguide," *Opt. Express.*, vol. 25, no. 26, pp. 33439–33450, Dec. 2017.

[17] F. Xu, C. Mei, J. H. Yuan, F. Li, Z. Kang, B. B. Yan, K. R. Wang, X. Z. Sang, X. Zhou, K. P. Zhong, and C. X. Yu, "Self-Similar Pulse Compression at Mid-Infrared Spectral Region in Tapered Tellurite Photonic Crystal Fiber," presented at Asia Communications and Photonics Conference (ACP) , Guangzhou, China, Nov. 11-13, 2017.

[18] Tonglei Cheng, Ryo Usaki, Zhongchao Duan, Weiqing Gao, Dinghuan Deng, Meisong Liao, Yasuhire Kanou, Morio Matsumoto, Takashi Misumi, Takenobu Suzuki, and Yasutake Ohishi, "Soliton self-frequency shift and third-harmonic generation in a four-hole As_2S_5 microstructured optical fiber," *Opt. Express.*, vol.22, no.4, pp.3740-3746, Feb. 2014.

[19] Q. Li, L. Liu, Z. X. Jia, G. S. Qin, Y. Ohishi, and W. P. Qin, "Increased red frequency shift in coherent mid-infrared supercontinuum generation from tellurite microstructured fibers," *J. Lightwave Technol.*, vol. 35, no. 21, pp. 4740–4746, Nov. 2017.

[20] Lizhu Li, Nurmemet Abdukerim, and Martin Rochette, "Mid-infrared wavelength conversion from As_2Se_3 microwires," *Opt. Lett.*, vol.42, no.3, pp.639-642, Feb. 2017.

[21] K. Saitoh, M. Koshiba, T. Hasegawa, and E. Sasaoka, "Chromatic dispersion control in photonic crystal fibers: Application to ultra-flattened dispersion," *Opt. Express.*, vol. 11, no. 8, pp. 843–852, Apr. 2003.

[22] D. Mogilevtsev, T. A. Birks, and P. S. Russell, "Group-velocity dispersion in photonic crystal fibers," *Opt. Lett.*, vol. 23, no. 21, pp. 1662–1664, Nov. 1998.

[23] J. M. Dudley, G. Genty, and S. Coen, "Supercontinuum generation in photonic crystal fiber," *Rev. Mod. Phys.*, vol. 78, no. 4, pp. 1135–1184, Oct. 2006.

[24] G. P. Agrawal, "Chapter 13 supercontinuum generation," in *Nonlinear fiber optics.* Fifth ed. San Francisco, CA, USA: Academic, 2013, pp. 388–426.

[25] X. Gu, L. Xu, M. Kimmel, E. Zeek, P. O'Shea, A. P. Shreenath, R. Trebino, and R. S. Windeler, "Frequency-resolved optical gating and single-shot spectral measurements reveal fine structure in microstructure-fiber continuum," *Opt. Lett.*, vol. 27, no. 13, pp. 1174–1176, Jul. 2002.

[26] T. North and M. Rochette, "Broadband self-pulsating fiber laser based on soliton self-frequency shift and regenerative self-phase modulation," *Opt. Lett.* Vol. 37, no. 14, pp. 2799–2801, Jul. 2012.

[27] J. M. Dudley, G. Genty, F. Dias, B. Kibler, and N. Akhmediev, "Modulation instability, Akhmediev Breathers and continuous wave supercontinuum generation," *Opt. Express.*, vol. 17, no. 24, pp. 21497–21508, Nov. 2009.

[28] M. S. Liao, X. Yan, W. Q. Gao, Z. C. Duan, G. S. Qin, T. Suzuki, and Y. Ohishi, "Five-order SRSs and supercontinuum generation from a tapered tellurite microstructured fiber with longitudinally varying dispersion," *Opt. Express.*, vol. 19, no. 16, pp. 15389–15396, Jul. 2011.

[29] J. H. V. Price, W. Belardi, T. M. Monro, A. Malinowski, A. Piper, and D. J. Richardson, "Soliton transmission and supercontinuum generation in holey fiber, using a diode pumped Ytterbium fiber source," *Opt. Express.* vol.10, no. 8, pp. 382–387, Apr. 2002.

[30] Hongxing Shi, Xian Feng, Fangzhou Tan, Peng Wang, and Pu Wang, "Multi-watt mid-infrared supercontinuum generated from a dehydrated large-core tellurite glass fiber," *Opt. Mater. Express*, vol.6, no.12, pp. 3967-3976, Dec. 2016.

[31] P. Domachuk, N. A. Wolchover, M. Cronin-Golomb, A. Wang, A. K. George, C.M.B. Cordeiro, J.C. Knight, and F. G. Omenetto, "Over 4000 nm Bandwidth of Mid-IR Supercontinuum Generation in sub-centimeter Segments of Highly Nonlinear Tellurite PCFs," *Opt. Express.*, vol.16, no.10, pp.7161-7168, May. 2008.

[32] J. M. Dudley and S. Coen, "Numerical simulations and coherence properties of supercontinuum generation in photonic crystal and tapered optical fibers," *IEEE J. Sel. Top. Quantum Electron.*, vol. 8, no. 3, pp. 651–659, Aug. 2002.

[33] C. Chaudhari, M. S. Liao, T. Suzuki, and Y. Ohishi, "Chalcogenide core tellurite cladding composite microstructured fiber for nonlinear applications," *J. Lightwave Technol.*, vol. 30, no. 13, pp. 2069–2076, Jul. 2012.

[34] V. I. Kruglov, A. C. Peacock, and J. D. Harvey, "Exact self-similar solutions of the generalized nonlinear Schrödinger equation with distributed coefficients," *Phys. Rev. Lett.*, vol. 90, no. 11, pp. 113902–2–4, Mar. 2003.

[35] V. I. Kruglov, A. C. Peacock, and J. D. Harvey, "Exact solutions of the generalized nonlinear Schrödinger equation with distributed coefficients," *Phys. Rev. E.*, vol. 71, no. 5, pp. 056619–1–10, May. 2005.

[36] G. Ghosh, "Sellmeier coefficients and chromatic dispersions for some tellurite glasses," *J Am. Ceram. Soc.*, vol. 78, no. 10, pp. 2828–2230, Jul. 1995.

[37] J. S. Wang, E. M. Vogel, and E. Snitzer, "Tellurite glass: a new candidate for fiber devices," *Opt. Mater.*, vol. 3, no. 3, pp. 187–203, Aug. 1994.

[38] X. Feng, W. H. Loh, J. C. Flanagan, A. Camerlingo, S. Dasgupta, P. Petropoulos, P. Horak, K. E. Frampton, N. M. White, J. H.V. Price, H. N. Rutt, and D. J. Richardson, "Single-mode tellurite glass holey fiber with extremely large mode area for infrared nonlinear applications," *Opt. Express.*, vol. 16, no. 10, pp. 13651–13656, Aug. 2008.

[39] J. Hu, C. R. Menyuk, L. B. Shaw, J. S. Sanghera, and I. D. Aggarwal, "Maximizing the bandwidth of supercontinuum generation in As_2Se_3 chalcogenide fibers," *Opt. Express.*, vol. 18, no. 7, pp. 6722–6739, Mar. 2010.

[40] G. P. Agrawal, "Chapter 6 optical pulse compression," in *Applications of nonlinear fiber optics*, 2ed. San Francisco, CA, USA: Academic, 2009, pp. 561–587.

[41] X. Yan, G. S. Qin, M. S. Liao, T. Suzuki, and Y. Ohishi, "Transient Raman response effects on the soliton self-frequency shift in tellurite microstructured optical fiber," *J. Opt. Soc. Am. B.*, vol. 28, no. 8, pp. 1831–1836, Aug. 2011.

[42] M. Liao, Z. Duan, W. Gao, X. Yan, T. Suzuki, and Y. Ohishi, "Dispersion engineering of tellurite holey fiber with holes formed by two glasses for highly nonlinear applications," *Appl. Phys. B.*, vol. 105, no. 5, pp. 681–684, Nov. 2011.

[43] J. G. Liu, T. H. Cheng, Y. K. Yeo, Y. X. Wang, L. F. Xue, Z. W. Xu, and D. W. Wang, "Light beam coupling between standard single mode fibers and highly nonlinear photonic crystal fibers based on the fused biconical tapering technique," *Opt. Express.*, vol. 17, no. 5, pp. 3115–3123, Mar. 2009.

[44] J. M. Dudley and S. Coen, "Coherence properties of supercontinuum spectra generated in photonic crystal and tapered optical fibers," *Opt. Lett.*, vol. 27, no. 13, pp. 1180–1182, Jul. 2002.

[45] G. Genty, M. Surakka, J. Turunen, and A. T. Friberg, "Complete characterization of supercontinuum coherence," *J. Opt. Soc. Am. B.*, vol. 28, no. 9, pp. 2301–2309, Sep. 2011.